PASJ: Publ. Astron. Soc. Japan **60**, 1051–1056, 2008 October 25

Japanese VLBI Network Observations of SiO Masers in the M-Type Giant IRC −10414

Kosuke UEDA,[1] Hiroshi IMAI,[1,2] Shuji DEGUCHI,[3] Ryuichi KAMOHARA,[4]
Toshihisa MAEDA,[1] Naoko MATSUMOTO,[1,5] and Toshihiro OMODAKA[1,2]
[1]*Graduate School of Science and Engineering, Kagoshima University, 1-21-35 Korimoto, Kagoshima, Kagoshima 890-0065*
[2]*Faculty of Science, Kagoshima University, 1-21-35 Korimoto, Kagoshima, Kagoshima 890-0065*
[3]*Nobeyama Radio Observatory, National Astronomical Observatory of Japan, Minamimaki, Minamisaku, Nagano 384-1305*
[4]*Mizusawa VERA Observatory, National Astronomical Observatory of Japan, 2-21-1 Osawa, Mitaka, Tokyo 181-8588*
[5]*Graduate School of Advanced Studies, 2-21-1 Osawa, Mitaka, Tokyo 181-8588*
hiroimai@sci.kagoshima-u.ac.jp

(Received 2008 March 5; accepted 2008 July 16)

Abstract

We present two-epoch maps of SiO masers ($v = 1$ and $v = 2$, $J = 1$–0) associated with the M-type star IRC −10414, which were obtained with the Japanese VLBI Network (JVN). The spatial and Doppler velocity distributions, and the intensity ratio of the $v = 1$ to $v = 2$ ($J = 1$–0) lines have significantly changed for eight years since our previous Very Long Baseline Array (VLBA) observation. The maser proper motions revealed by these two-epoch observations with an interval of one month are quite random and too fast to be explained by ballistic motions of the maser clumps. The maser distributions seen in the present observations cannot be explained by a rotating-infalling ring model implied in the previous work. We discuss the kinematical relation between the SiO and H_2O masers in IRC −10414. In the present observations, the scale sizes of SiO $v = 1$ and $v = 2$ masers in IRC −10414 were roughly equal, as observed in typical Mira variables.

Key words: masers — stars: AGB and post-AGB — stars: circumstellar matter — stars: individual (IRC −10414)

1. Introduction

A star with an initial mass of 1–8$M_\odot$ finally passes through the asymptotic giant branch (AGB) phase, while undergoing the most copious mass loss, and eventually evolves into a white dwarf with an accompanying planetary nebula (PN). There still exists a missing link in the mass-loss history between the AGB and post-AGB phases. It has been stated that many young PNe exhibit bipolar morphologies or large deviations from spherical symmetry, whereas the central stars should be spherically symmetric (e.g., Aaquist & Kwok 1991; Sahai & Trauger 1998). Such PN asymmetry may be caused by asymmetric mass loss on the stellar surface, but it cannot be directly observed, because the central stars are heavily obscured by the gas and dust ejected from the stars, themselves. Many oxygen-rich AGB stars often harbor SiO, H_2O, and OH maser emission consisting of many compact maser features, whose proper motions are able to be measured with great accuracy achieved in very long baseline interferometry (VLBI). The SiO maser emitting regions are located at distances of between 10^{11} m and 10^{12} m from the stellar surface, and are the closest to the host AGB stars in the three species of masers. Therefore, SiO masers have been used to resolve the complicated structures seen around the central star.

In the present paper, we present maps of SiO maser emission in IRC −10414 obtained with the Japanese VLBI Network (JVN) during two epochs. IRC −10414 (GL 2139, OH 17.55−0.13, IRAS 18204−1344) is classified as an M8 giant (Lockwood 1985) and as a source of bright OH, H_2O, and SiO maser emission (Engels 1979; Ukita & Goldsmith 1984). The distance to IRC −10414, the luminosity, and the stellar mass-loss rate have been estimated to be $D \approx 700$ pc, $L_* \approx 10^4 L_\odot$, and $\dot{M} = 4 \times 10^{-6} M_\odot \mathrm{yr}^{-1}$ (Jura & Kleinmann 1989). H_2O maser emission in IRC −10414 was found by Kleinman, Sargent, and Dickinson (1978), and mapped by Lada et al. (1981). Recently, Maeda et al. (2008) revealed the three-dimensional velocity field of H_2O masers exhibiting a bipolar outflow. They reestimated the distance to be $D =$ 2–3 kpc, resulting in $L_* = 9$–$20 \times 10^4 L_\odot$ and $\dot{M} = 4$–$6 \times 10^{-5} M_\odot \mathrm{yr}^{-1}$, suggesting that IRC −10414 is a supergiant rather than a red giant.

The SiO maser emission from IRC −10414 was mapped by Imai, Deguchi, and Miyoshi (1999) (IDM99 hereafter), and was found to exhibit a possible rotating ring or disk structure, whose diameter is ~ 14 mas with a rotation axis at a position angle of $\sim 3°$, measured from north to east. This axis is almost parallel to the major axis of the outflow found in the H_2O masers (Maeda et al. 2008). However, to reveal the true spatio-kinematical structure of an SiO maser source, especially if it is expected to be dominated by the stellar gravity, the maser source should again be observed several years later (cf. for IK Tau, Boboltz & Diamond 2005; Matsumoto et al. 2008). In fact, in the present observations, the rotating disk structure in IRC −10414 was not revealed.

Table 1. Parameters of the JVN observations and the data reduction.

Code	Observation epoch in 2006	Duration (hr)	1σ level noise (Jy beam^{-1})	Synthesized beam* 42.8 GHz	Synthesized beam* 43.1 GHz	$N_{\rm features}$† $v=2$	$N_{\rm features}$† $v=1$
r06080b	March 21	6.5‡	4.1	0.85×0.80, $-32°$	0.84×0.80, $-33°$	5	14
r06117a	April 27	6.8§	2.5	1.05×0.85, $-8°$	1.04×0.85, $-32°$	7	14

* Synthesized beam made in natural weight; major and minor axis lengths in units of mas and a position angle.
† Number of detected maser features.
‡ Data from the VERA Iriki antenna were completely invalid because of too high system noise temperatures in the whole scans.
§ Data from the VERA Ishigaki antenna were almost invalid because of too high system noise temperatures in most of the scans.

2. Observations and Data Reduction

We simultaneously observed two SiO maser lines ($v = 1$ and $v = 2$, $J = 1$–0) in IRC −10414 [RA(J2000.0) = $18^{\rm h}23^{\rm m}17^{\rm s}.866$, Dec(J2000.0) = $-13°42'47''.67$] on 2006 March 21 and April 27, using six telescopes of the JVN; the four 20 m telescopes of the VLBI Exploration of Radio Astrometry (VERA); the 45 m telescope of Nobeyama Radio Observatory (NRO); and the 34 m telescope of the National Institute of Communications Technology (NICT). In each epoch, the observation was made for ~ 7 hr, including scans of calibrators (NRAO 530 and OT 081). In the present paper, 43.122079 GHz and 42.820582 GHz are adopted as rest frequencies for the SiO $v = 1$ and $v = 2$ ($J = 1$–0) transitions, respectively. The signals, received in left-hand circular polarization, were digitized in four levels, filtered into two base band channels with a band width of 16 MHz each (covering $\sim 111\,{\rm km\,s^{-1}}$ in velocity), and recorded with the SONY DIR1000 recorder at a rate of 128 Mbits s^{-1}. Data correlation was made with a Mitaka FX correlator. The accumulation period of the correlation was set to 1 s. The correlation outputs consisted of 512 velocity channels, yielding a velocity spacing of $\sim 0.22\,{\rm km\,s^{-1}}$.

To obtain image cubes for the maser source, data reduction was made using the NRAO AIPS package in normal procedures (see also Matsumoto et al. 2008). Fringe fitting and self-calibration procedures were made for using visibilities in a Doppler velocity channel at $V_{\rm LSR} = 40.7\,{\rm km\,s^{-1}}$, including a bright maser spot (velocity component). The solutions were applied to data in other velocity channels. Note that after applying these calibrations, information about the absolute positions is lost from the maser image cubes. A typical size of the synthesized beam was 1 milliarcsecond (mas) in the two observations. In order to identify and parameterize maser components, two-dimensional Gaussian functions were fitted to the emission above a signal-to-noise ratio cutoff of 5 in each spectral channel using the AIPS task SAD. Identification of the position of an SiO maser feature, or a physical gas clump composed of several velocity components within ~ 2 mas in position and $\sim 1\,{\rm km\,s^{-1}}$ in Doppler velocity, is defined as a velocity-integrated brightness peak in the feature. The relative position accuracy of a maser feature was ranged over 0.002–0.420 mas, depending on the signal-to-noise ratio. However, the accuracy may be much worse when taking into account the extended structure of SiO maser emission invisible in the present VLBI observations. Note that the maser features were identified when they were found to occupy two or more adjacent spectral channels ($\Delta V \geq 0.4\,{\rm km\,s^{-1}}$). Table 1 gives some parameters of the observations and data reduction.

3. Results and Discussion

3.1. Spatial and Velocity Distributions of the SiO Masers

Table 2 gives parameters of the detected SiO maser features associated with IRC −10414 in the present observations. Two upper panels in figure 1 [a ($v = 1$) and b ($v = 2$)] show velocity-integrated intensity maps of SiO $v = 1$ and $v = 2$ ($J = 1$–0) transitions between the two epochs. Figure 2 shows the distributions of the Doppler velocities of the maser features with respect to the local standard of rest (LSR), in which all maser features detected in all the observations are plotted. An LSR velocity gradient from east to west, as can be seen in IDM99, is marginally found. However, there are many maser features spread in the north–south direction as well. This direction corresponds to the direction of the major axis of a bipolar outflow found for the H_2O masers (Maeda et al. 2008).

By finding maser feature pairs located at almost the same relative position (within 1 mas) and LSR velocity (within $0.5\,{\rm km\,s^{-1}}$), we found 13 and 3 proper motions in $v = 1$ and $v = 2$ maser features, respectively. Note that the reliability of the proper-motion measurement is poor because they were derived from only two epochs of observations, separated by about one month. The proper motions are indicated by arrows in figure 2. If the distance to IRC −10414 is adopted to be 2 kpc (Maeda et al. 2008), the linear velocities of the maser features *apparently* achieve up to $\sim 110\,{\rm km\,s^{-1}}$. Even if we assume a distance of 710 pc (Jura & Kleinmann 1989), the proper motions are converted to $\sim 40\,{\rm km\,s^{-1}}$. The derived linear velocities are much larger than the LSR velocity width of only 5–15 km s^{-1} (see also IDM99). Very likely, we are looking at the *Christmas tree effect*, in which only the physical conditions for preferentially lighting up the masers change in certain regions of the circumstellar envelope. In this case, we are incorrectly tracing the same maser feature from one epoch to another. To exactly identify true proper motions, we need one more data point for each feature by performing the third epoch of observation. Here, we suppose that only small proper motions ($\lesssim 5\,{\rm mas\,yr^{-1}}$) may trace real ballistic motions

Table 2. Parameters of all detected maser features.

V_{LSR} (km s^{-1})	X (mas)	σ_X	Y (mas)	σ_Y	I_{int}*	Size (mas)	ΔV† (km s^{-1})
$v = 1$ emission on 2006 March 21							
38.31	12.988	0.003	−1.821	0.004	0.77	0.64	1.96
38.16	12.241	0.002	−2.141	0.006	0.48	0.25	1.30
39.07	5.977	0.009	0.285	0.012	0.37	0.43	2.61
41.67	−1.266	0.021	5.279	0.011	0.42	0.43	1.09
40.71‡	−0.166	0.001	−0.051	0.001	4.69	1.41	1.74
41.12	−0.287	0.003	−6.309	0.002	2.35	0.70	1.74
39.41	5.977	0.014	−5.782	0.018	0.55	0.49	1.96
41.68	7.876	0.020	−7.554	0.018	1.06	0.56	2.17
40.60	7.338	0.050	−14.489	0.036	1.14	1.05	3.04
39.61	6.546	0.002	−13.364	0.003	1.32	0.92	1.30
41.87	8.241	0.006	−13.579	0.007	1.25	0.58	1.74
41.43	7.523	0.002	−13.671	0.002	1.80	0.55	1.96
41.56	9.091	0.009	−13.074	0.009	1.12	0.42	1.96
41.49	6.005	0.042	−19.663	0.414	1.19	1.91	2.39
$v = 2$ emission on 2006 March 21							
41.79	0.293	0.037	6.393	0.039	1.28	0.48	1.31
41.35‡	−0.126	0.013	−0.035	0.011	7.33	0.92	1.75
41.35	−0.393	0.149	−6.289	0.043	0.92	0.75	1.97
41.13	4.585	0.047	−10.423	0.061	0.68	0.35	2.63
42.66	7.765	0.047	−12.804	0.059	0.75	0.37	0.44
$v = 1$ emission on 2006 April 27							
37.88	12.250	0.056	−2.809	0.010	0.55	1.31	1.09
38.48	12.489	0.006	−2.136	0.008	0.66	0.65	0.65
37.74	6.153	0.004	0.306	0.005	0.59	0.54	1.52
42.40	−1.220	0.007	4.261	0.013	0.59	0.39	1.09
40.75‡	−0.059	0.001	−0.002	0.001	2.11	1.40	2.17
40.32	0.780	0.021	−5.613	0.022	0.81	0.86	2.17
38.04	5.987	0.011	−5.810	0.011	0.46	0.34	3.04
41.67	8.608	0.024	−7.746	0.050	0.62	0.64	4.13
39.77	6.985	0.011	−12.956	0.015	0.42	0.39	0.65
40.36	7.965	0.027	−14.609	0.033	0.48	0.76	5.21
43.61	8.396	0.005	−13.261	0.006	0.62	0.76	1.09
41.16	7.574	0.001	−13.653	0.002	1.01	0.74	3.26
41.96	7.440	0.001	−13.553	0.001	0.55	0.51	3.04
41.22	7.982	0.014	−19.159	0.073	0.57	0.93	4.13
$v = 2$ emission on 2006 April 27							
40.26	7.600	0.171	13.500	0.335	0.04	0.02	1.31
40.26	−0.754	0.033	7.237	0.035	0.25	0.36	2.41
39.61	6.139	0.049	0.263	0.054	0.23	0.52	3.06
41.5871‡	−0.004	0.003	0.005	0.003	6.25	0.93	1.53
38.29	−0.003	0.144	−7.536	0.076	0.10	0.47	1.53
39.83	5.084	0.043	−10.554	0.052	0.12	0.24	2.63
36.54	8.335	0.037	−12.984	0.058	0.18	0.38	1.09

* Velocity-integrated peak intensity of the feature in units of Jy km s^{-1} beam^{-1}.
† Full velocity width with maser emission.
‡ Maser feature containing the maser spot in the phase-reference velocity channel.

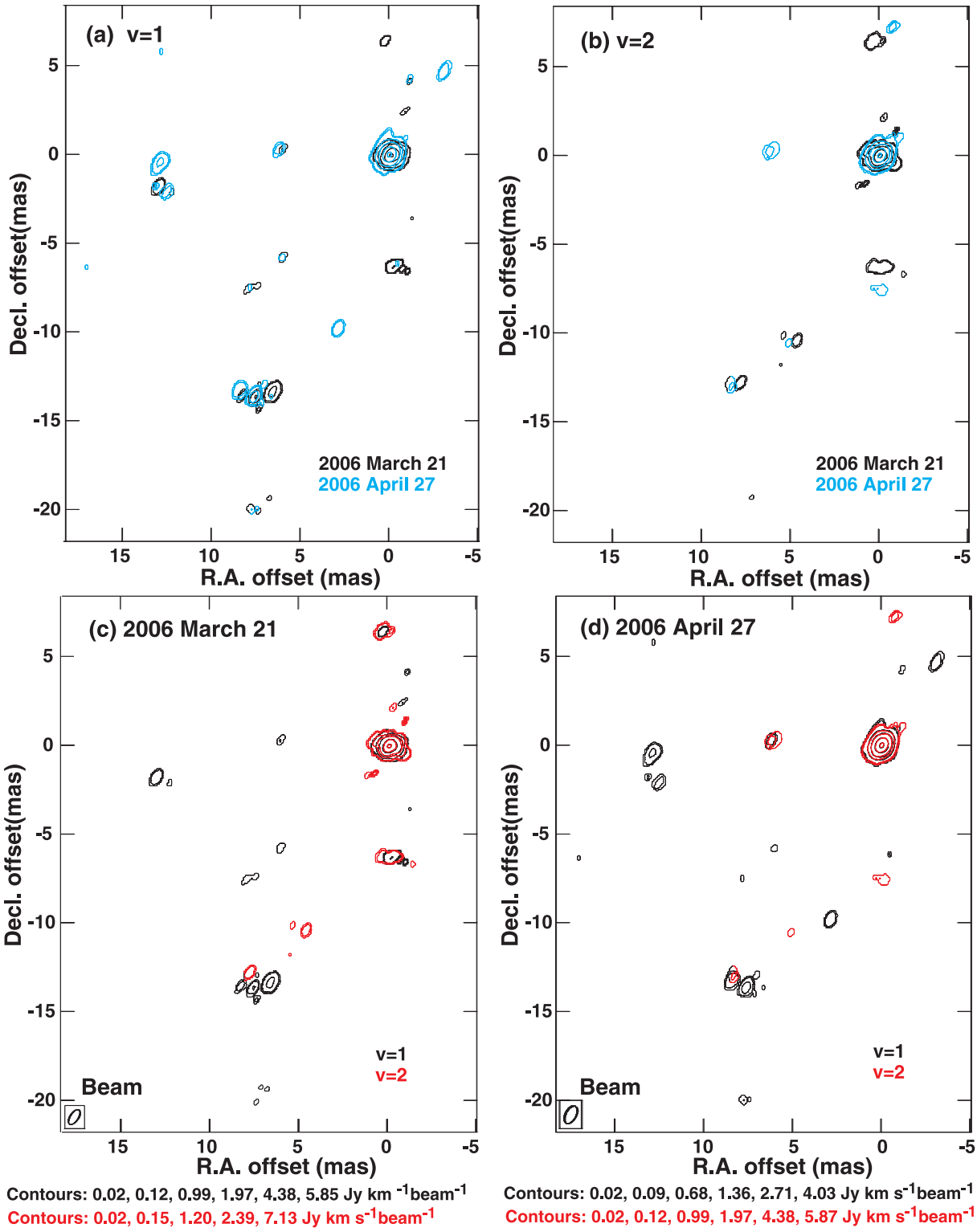

Fig. 1. Velocity-integrated intensity contour maps of the SiO $v = 1$ and $v = 2$ ($J = 1$–0) emission lines seen at the two epochs. Only maser emission higher than 7σ, not 5σ, was collected. Here, the noise level was independently measured in each spectral channel map. The map origin is located at the position of the reference maser spots of $v = 1$ and $v = 2$ lines at $V_{\rm LSR} = 40.7\,{\rm km\,s^{-1}}$. Contour levels of the maser intensity are shown in panels (c) and (d). (a) Comparison of the $v = 1$ maps between the first (black) and second (cyan) epochs. (b) Same as (a), but for the $v = 2$ map. (c) Comparison between the $v = 1$ (black) and $v = 2$ (red) maps at the first epoch. (d) Same as (c), but at the second epoch.

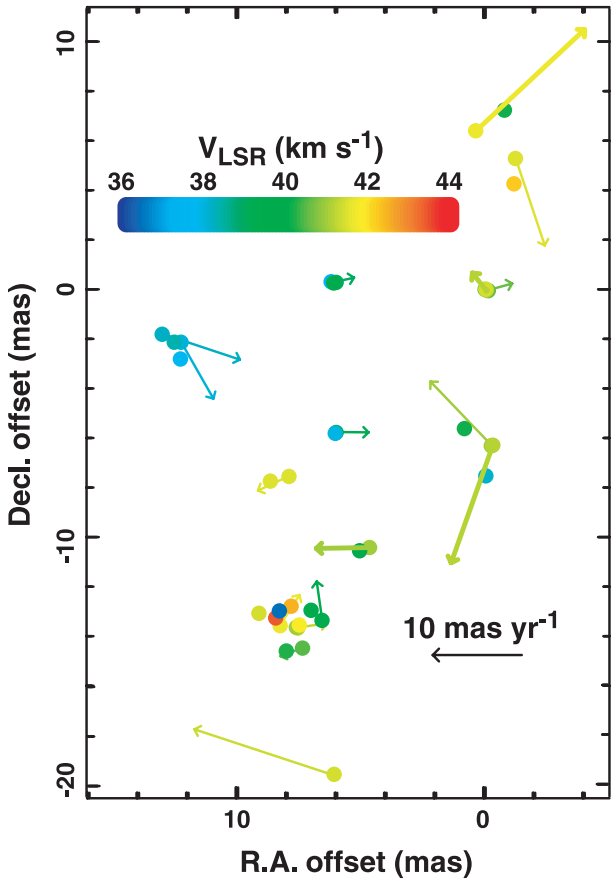

Fig. 2. Composite map and proper-motion distribution of the IRC −10414 SiO masers. The map origin is located at the position of the reference maser spots of $v = 1$ and $v = 2$ lines at $V_{\rm LSR} = 40.7 {\rm km\,s^{-1}}$. In the map, all maser features detected at least at one epoch are displayed. The feature color indicates the LSR velocity shown in the color scale at the top, which ranges from $36 {\rm km\,s^{-1}}$ to $44 {\rm km\,s^{-1}}$. An arrow indicates the location and the relative proper-motion vector of a maser feature with the mean proper motion subtracted. Thick and thin arrows show proper motions for the $v = 2$ and $v = 1$ maser features, respectively.

of maser gas clumps. There are three $v = 1$ maser features that meet the criterion of a possible real proper motion. We note that these three features were apparently moving from east to west. These motions are roughly perpendicular to the bipolar outflow found in the H_2O maser (Maeda et al. 2008), implying a rotation motion around the central star. Assuming a Keplerian rotation for these three features, as suggested by IDM99, we derive a rotation velocity of $18 {\rm km\,s^{-1}}$ and the mass of the central star being $3.2 M_\odot$. These values are still realistic, but smaller than those expected from the suggestion that the central star should be a supergiant (Maeda et al. 2008). We cannot also explain other SiO maser features using this hypothesis.

On the other hand, Matsumoto et al. (2008) also show, based on multiepoch VLBI observations of SiO masers in IK Tauri, that it is quite difficult to reliably trace ballistic motions of individual SiO maser features on a short time scale, like that made in the present observations. Instead, they found that spoke-shaped SiO maser features may reflect possible dynamical motions of the maser features. In the present data, there was no maser feature exhibiting such a spoke-shaped structure due to insufficient angular resolution. Instead, we found such maser features in the IRC −10414 SiO masers in the previous observation (IDM99). Using the same data as those in IDM99, the distribution of individual maser spots is plotted in figure 3. We find that some of the spoke-shaped features of $v = 1$ emission [a, d, e(west side), f, and h] elongated radially from the center of the maser feature distribution, and had LSR velocity gradients that suggested deceleration, as demonstrated by Matsumoto et al. (2008). Thus, it is likely that the maser features are moving in the radial direction from the center of the maser distribution, rather than rotating around the center.

We also note that the total LSR velocity width is larger than those typically found in Mira variables ($\lesssim 10 {\rm km\,s^{-1}}$), but comparable to those found in supergiants (see figure 3). This supports the suggestion that IRC −10414 is a supergiant (Maeda et al. 2008). We also suppose a biconically expanding flow for the spatiokinematical structure of SiO masers, as adopted for W 43A (Imai et al. 2005). This model suggests the existence of biconical cavities of the SiO maser feature locations, but such a structure was not so clear in IRC −10414. It is speculated that the bipolar outflow of IRC −10414 is not so fast or so developed that it could create such biconical cavities in the circumstellar envelope. The circumstellar envelope of IRC −10414 may be in the same condition as that of WX Psc, where the SiO maser distribution still exhibits a circular ring (Soria-Ruiz et al. 2004), while a bipolar outflow has just been launched (Inomata et al. 2007).

3.2. *Spatial Coincidence of the SiO $v = 1$ and $v = 2$ Masers*

The two lower panels (c and d) in figure 1 show maps of maser features of the SiO $v = 1$ and $v = 2$ ($J = 1$–0) transitions associated with IRC −10414 in the two epochs. The positions of a few bright $v = 2$ features fall close to those of the corresponding $v = 1$ features within a few mas, although the number of detected spots is larger in the $v = 1$ ($J = 1$–0) transition than in the $v = 2$ ($J = 1$–0) transition. This tendency is consistent with that found in typical SiO masers around Mira variables. Desmurs et al. (2000), Soria-Ruiz et al. (2004), and Yi et al. (2005) have shown that $v = 2$ emission is always located closer to the central star, on the same scale as that mentioned above. A similar tendency may be found in the present observations, but more maser features are necessary for clear confirmation.

Note that the SiO masers in IRC −10414 have the unique property that the flux density ratio between $v = 1$ and $v = 2$ ($J = 1$–0) lines has changed by two orders of magnitude for eight years. In many stellar SiO masers, although the ratio is weakly correlated with the infrared color of the circumstellar envelope (Nakashima & Deguchi 2007), it is typically stable in each star (e.g., Pardo et al. 2004). According to unpublished data of SiO maser emission in IRC −10414, obtained with VERA single-dish observations, the flux ratio was close to unity when the present JVN observations were made. On the other hand, the previous observation by IDM99 could not map the $v = 2$ emission because of its weakness. A similar situation is found in the SiO masers in W 43A (Imai et al. 2005) and IRAS 19312+1950 (Nakashima et al. 2008). These stars may be either at the last stage of the AGB phase or at the initial stage of the post-AGB phase, and have cold IRAS colors (Nakashima

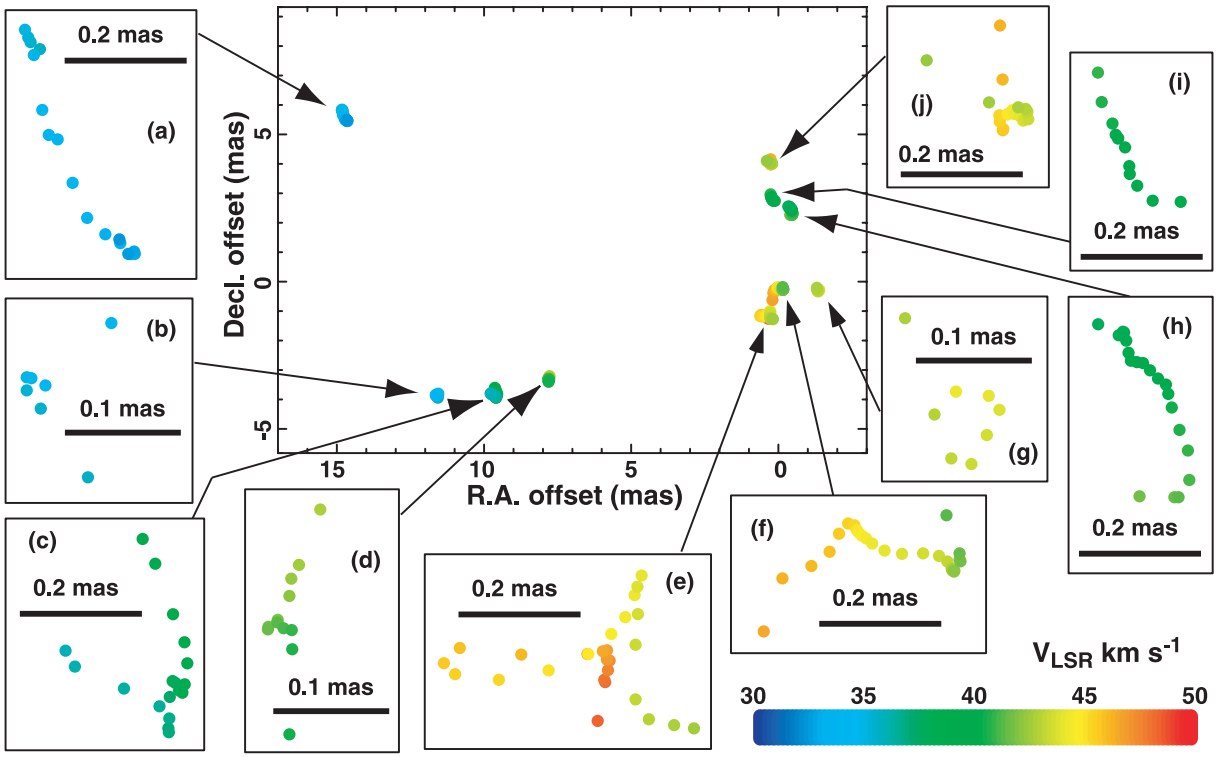

Fig. 3. Enlarged view of alignments of SiO $v = 1$ maser spots (velocity components) in IRC −10414 found by Imai, Deguchi, and Miyoshi (1999). The feature color indicates the LSR velocity shown in the color scale at the right bottom corner, which ranges from 30 km s^{-1} to 50 km s^{-1}.

& Deguchi 2003). They are also expected to exhibit the most active mass loss in their evolution. A temporal increase in the mass-loss rate of IRC −10414, therefore, is one possible explanation for the temporal flux-ratio deviation from unity. Note that, however, IRC −10414 has a relatively hot IRAS color [$\log(F_{25\mu m}/F_{12\mu m}) = -0.18$, $H - K = 0.69$], which is inconsistent with the IRAS colors of the three above-mentioned sources. Also note that the distributions of $v = 1$ and $v = 2$ lines well resemble each other, even around supergiants (e.g., VY CMa: Miyoshi et al. 1994).

The authors would like to thank all staff members of NRO, NICT, and VERA for their assistance concerning the present JVN observations and data correlation. They also thank students of Kagoshima University. They deeply appreciate Drs. Javier Alcolea and David Boboltz for carefully reading the manuscript and providing critical comments. T. O. and H. I., and H. I. have been financially supported by Grants-in-Aid for Scientific Research from Japan Society for the Promotion of Science (17340055, and 18740109 and 20540234, respectively).

References

Aaquist, O. B., & Kwok, S. 1991, ApJ, 378, 599
Boboltz, D. A., & Diamond, P. J. 2005, ApJ, 625, 978
Desmurs, J. F., Bujarrabal, V., Colomer, F., & Alcolea, J. 2000, A&A, 360, 189
Engels, D. 1979, A&AS, 36, 337
Imai, H., Deguchi, S., & Miyoshi, M. 1999, PASJ, 51, 587 (IDM99)
Imai, H., Nakashima, J., Diamond, P. J., Miyazaki, A., & Deguchi, S. 2005, ApJ, 622, L125
Inomata, N., Imai, H., & Omodaka, T. 2007, PASJ, 59, 799
Jura, M., & Kleinmann, S. G. 1989, ApJ, 341, 359
Kleinman, S. G., Dickinson, D. F., & Sargent, D. G. 1978, AJ, 83, 1206
Lada, C. J., Blitz, L., Reid, M. J., & Moran, J. M. 1981, ApJ, 243, 769
Lockwood, G. W. 1985, ApJS, 58, 167
Maeda, T., et al. 2008, PASJ, 60, 1057
Matsumoto, N., et al. 2008, PASJ, 60, 1039
Miyoshi, M., Matsumoto, K., Kameno, S., Takaba, H., & Iwata, T. 1994, Nature, 371, 395
Nakashima, J., & Deguchi, S. 2003, PASJ, 55, 229
Nakashima, J., & Deguchi, S. 2007, ApJ, 669, 446
Nakashima, J., Deguchi, S., Imai, H., & Kemball, A. 2008, in Proc. IAU Symp. 251 in press
Pardo, J. R., Alcolea, J., Bujarrabal, V., Colomer, F., del Romero, A., & de Vicente, P. 2004, A&A, 424, 145
Sahai, R., & Trauger, J. T. 1998, AJ, 116, 1357
Soria-Ruiz, R., Alcolea, J., Colomer, F., Bujarrabal, V., Desmurs, J.-F., Marvel, K. B., & Diamond, P. J. 2004, A&A, 426, 131
Ukita, N., & Goldsmith, P. F. 1984, A&A, 138, 194
Yi, J., Booth, R. S., Conway, J. E., & Diamond, P. J. 2005, A&A, 432, 531